Fermi surface reconstruction in $CeTe_2$ induced by charge density waves investigated via angle resolved photoemission

J.-S. Kang,[1,*] D. H. Kim,[1] H. J. Lee,[1] Jihoon Hwang,[1] Han-Koo Lee,[2] H.-D. Kim,[2] B. H. Min,[3] K. E. Lee,[3] Y. S. Kwon,[3] J. W. Kim,[4] Kyoo Kim,[4] B. H. Kim,[4] and B. I. Min[4,†]

[1]*Department of Physics, The Catholic University of Korea, Bucheon 420-743, Korea*

[2]*Pohang Accelerator Laboratory, Pohang University of Science and Technology, Pohang 790-784, Korea*

[3]*Department of Physics, Sungkyunkwan University, Suwon 440-746, Korea*

[4]*Department of Physics, Pohang University of Science and Technology, Pohang 790-784, Korea*

(Received 3 January 2012; published 10 February 2012)

Electronic structures of a charge-density wave (CDW) system $CeTe_{2-x}Sb_x$ ($x = 0, 0.05$) have been investigated by employing angle-resolved photoemission spectroscopy (ARPES) and the first-principles electronic and phonon band-structure methods. The observed Fermi surface (FS) agrees very well with the calculated FS for the undistorted $CeTe_2$ both in shapes and sizes. The metallic states crossing the Fermi level (E_F) are observed in ARPES even in the CDW state. The carriers near E_F have mainly the Te(1) $5p$ character, with a negligible contribution from Ce $4f$ states. The supercell (shadow) bands and the corresponding very weak FSs are found to arise from band folding due to the interaction of Te(1) layers with Ce-Te(2) layers. We found that the CDW modulation vector is along Γ-X ($\mathbf{Q}_{CDW} \approx X$), which is not coincident with the most prominent FS nesting vector.

DOI: 10.1103/PhysRevB.85.085104 PACS number(s): 71.45.Lr, 71.18.+y, 71.20.−b, 79.60.−i

I. INTRODUCTION

$CeTe_2$ is known as a charge-density wave (CDW) system having a high CDW transition temperature of $T_{CDW} \sim 1000$ K, and intriguingly the CDW state coexists with magnetism and also with superconductivity ($T_C = 2.7$ K) under pressure.[1] $CeTe_2$ crystallizes in the quasi-two-dimensional layered Cu_2Sb-type tetragonal structure with two types of Te sites: Te(1) and Te(2). Te(1) atoms form planar square sheets, which are sandwiched along the c axis by the corrugated double layers of Ce and Te(2) atoms (Fig. 1). The ionic configuration of $CeTe_2$ is considered to be $Ce^{3+}Te(2)^{2-}Te(1)^{1-}$, so that hole carriers are produced in Te(1) sheets.[2] Then the square net of Te(1) would be easily distorted by the Peierls-like mechanism[3] due to the partial filling. Underneath this picture is the assumption of trivalent Ce^{3+} states.[4] Band-structure calculations indicate that the CDW instability occurs due to the nesting between the Fermi surfaces in Te(1) square sheets in the a-b plane,[5–7] which was supported experimentally.[8] However, the relevant CDW modulation vector has not been identified.

Due to the difficulty in growing high-quality single crystals appropriate for the angle-resolved photoemission spectroscopy (ARPES) study, there have been only a few ARPES reports on $CeTe_2$, which studied the Fermi-surface (FS) topology in the CDW state.[9,10] This is in contrast to similar CDW systems, $LaTe_2$ and RTe_3 (where R indicates a rare-earth element), for which more complete ARPES studies have been reported.[9,11,12] Shin *et al.*[9] reported that the FS topology of $CeTe_2$ in the k_x-k_y plane is different from that of $LaTe_2$.[11] They conjectured that the CDW gap E_g is larger than $\geqslant$600 meV and that the magnitude of E_g varies around the FS. This minimum value of $E_g \approx 600$ meV is much larger than $E_g \approx 100$ meV, found in another ARPES study.[2] Ito *et al.*[10] examined the FS along the k_z axis and observed some intensity modulation in the spectral weight at FS. Therefore, no good understanding has been made yet for the CDW state of $CeTe_2$.

As shown in Fig. 1(a), Te(1) ions in $CeTe_2$ form the planar square lattices, which are sandwiched by the double layers of Ce and Te(2) ions. Due to the underlying Ce-Te(2) layer, the unit cell of Te(1) square lattices is doubled in $CeTe_2$ ($\sqrt{2} \times \sqrt{2}$) [see Fig. 1(b)]. Accordingly, the Brillouin zone (BZ) is reduced to a half of that of Te(1) square lattices, and thereby the bands are folded into the reduced BZ to produce the supercell (shadow) bands. In reality, the periodicity of the potential in the Te(1) layer depends on the hybridization strength between Te(1) and Ce-Te(2) layers. If the hybridization strength is small, the electronic structure of Te(1) ions would keep the two-dimensional nature of the planar square lattices. Otherwise, it will have a three-dimensional (3D)-like nature.

The FSs, denoted with dotted lines in Fig. 1(b), come from those shadow bands. The natural question concerns the role of Ce $4f$ and Te $5p$ electrons in $CeTe_2$. This includes the following issues: (i) whether the FS topology and the CDW state of $CeTe_2$ are the same as those of the non-f electron CDW system of $LaTe_2$; (ii) how large is the effect of the band folding, arising from the interaction between Te(1) and Ce-Te(2) layers, on the FS of Te(1) sheets; and (iii) what is the CDW modulation vector, $\mathbf{Q}_{CDW}$. We have resolved these questions by performing careful ARPES measurements for high-quality stoichiometric single crystals of $CeTe_{2-x}Sb_x$ ($x = 0, 0.05$) and also by carrying out first-principles electronic and phonon band calculations.

II. EXPERIMENTAL AND CALCULATIONAL DETAILS

High-quality $CeTe_{2-x}Sb_x$ single crystals having very low residual resistivity were grown by using the self-fluxed Bridgeman method.[13] The quality and the orientation of the single crystal were checked by Laue patterns. ARPES experiments were carried out at the 3A1 beamline of the Pohang Light Source with a beam size of <50 μm and using a Scienta SES-2002 electron energy analyzer. Single crystals were cleaved *in situ* at $T \sim 30$ K under pressure better than 5×10^{-11} Torr, which exposed the (001) surfaces. The Fermi level and the overall instrumental resolution of the system were determined from the Fermi edge of an evaporated Cu metal.

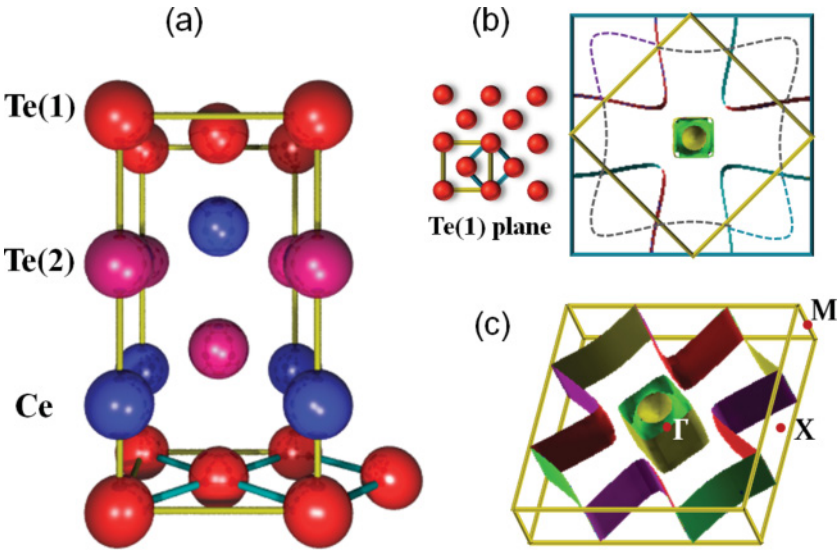

FIG. 1. (Color online) (a) Tetragonal crystal structure of $CeTe_2$ in the non-CDW phase. (b) Unit cell of the Te(1) square net doubled in tetragonal $CeTe_2$; thus, the Brillouin zone (BZ) of Te(1) sheets (the outer square) is reduced to half (the inner square); the FS in the outer BZ is folded into the inner BZ. (c) FS of $CeTe_2$ in the tetragonal BZ of the non-CDW phase; Γ, X, and M represent $\mathbf{k} = (0,0,0)$, $\frac{2\pi}{a}(1/2, 0, 0)$, and $\frac{2\pi}{a}(1/2, 1/2, 0)$, respectively.

The energy resolution (ΔE) and the momentum resolution (Δk) were set to be $\Delta E \sim 80$ meV and $\Delta k \approx 0.01 \text{Å}^{-1}$, respectively, at $h\nu \sim 110$ eV.

For band calculations, we have employed the *ab initio* full-potential linearized augmented band calculations in the generalized gradient approximation (GGA), including the Coulomb interaction U between Ce $4f$ electrons and the spin-orbit interaction.[14] To analyze the ARPES data of $CeTe_2$, we have "unfolded" the calculated band structure, by employing the band-unfolding scheme that was recently developed by Ku *et al.*[15] In this scheme, the Kohn-Sham states are projected into the Wannier states. Then, using the relation between the "large" and "small" unit cells, one can reconstruct the Wannier states for the small unit cell out of those for the large unit cell of $CeTe_2$. In this way, one can separate out the shadow bands from the main bands in the large BZ. The intensity of the Te(1) supercell band is proportional to the interaction between the Te(1) layer and the underlying Ce-Te(2) layer. If the interaction is weak, it results in the weakening of the weights of the supercell-folded bands and the corresponding Fermi surface (FS).

In order to perform the phonon-dispersion calculation, we have used the density-functional perturbation theory, as implemented in QUANTUM-ESPRESSO (QE).[16] The self-consistent electronic structure calculations were carried out in the GGA by using the pseudopotential band method that is also implemented in QE. A $N_k = 20 \times 20 \times 10$ grid was used for the electronic structure. The dynamical matrices are obtained on the $N_q = 4 \times 4 \times 2$ phonon-momentum grid. In these calculations, we employed the cutoffs of 408 and 1632 eV for the wave functions and the charge density, respectively.

III. RESULTS AND DISCUSSION

Figures 2(a) and 2(b) show the first-derivative constant energy (CE) maps of $CeTe_2$ and $CeTe_{1.95}Sb_{0.05}$ versus the initial-state energy (E_i) of $-1.2 \leqslant E_i \leqslant -0.2$ eV, obtained at $T \sim 30$ K with $h\nu \approx 115$ eV. In plotting each CE map, the spectral intensity of $E_i \pm 100$ meV was integrated. This figure shows that the CE maps of $x = 0$ and 0.05 are essentially the same in their shapes, sizes, and energy-dependent behavior[17] but that those of $x = 0.05$ are sharper than those of $x = 0$.

The fourfold symmetry is observed in the CE maps and the FS [Fig. 2(e)], which is shown more clearly in the CE map for $E_i = -1.0$ eV [Fig. 2(c)], which was obtained from a different cleave. Two diamond-shaped contours are observed in the FS map, which is similar to the case of $LaTe_2$.[11] This finding implies that Ce $4f$ electrons hardly contribute to the states near the Fermi level (E_F). Note that the inner diamond FS is clearly seen in both $x = 0$ and 0.05, in contrast to the case of Ref. 9. With increasing $|E_i|$, the size of the inner diamond increases, while that of the outer diamond remains nearly the same. This energy-dependent behavior is consistent with that of the calculated FSs, shown in Fig. 2(d). According to band calculations, the overall FS structures are the same between $CeTe_2$ and $LaTe_2$, except for the additional electron FS around Z in the $k_z = \pi/c$ plane of $CeTe_2$. This FS is dispersive along the k_z axis, in agreement with the report by Ito *et al.*[10] This feature indicates that the 3D nature is stronger in $CeTe_2$ than in $LaTe_2$.

Figure 2(e) shows the FS of $CeTe_{1.95}Sb_{0.05}$, drawn in the periodic zone scheme. This FS map was obtained by integrating the ARPES spectra for $E_F \pm 50$ meV ($E_F \equiv 0$ eV). The existence of the FS implies that there remain metallic states even below the CDW transition with the remnant ungapped FS. This conclusion is supported by the calculated FS, shown in Fig. 2(f), where the experimental and calculated FSs are compared. The former is obtained by connecting the partially ungapped FSs in Fig. 2(e), and the latter is calculated for the non-CDW phase. The experimental and calculated FSs are very similar to each other in both sizes and shapes, supporting the fact that the measured FS represents the FS of the non-CDW phase of $CeTe_2$. This comparison reveals two important features. First, the FS nesting is confirmed in $CeTe_2$. Second, the opening of the CDW gaps occurs only partially in some part of the FS, which is consistent with the semimetallic nature of $CeTe_2$.[2,18,19]

Recently, Johannes and Mazin[20] showed that the FS nesting does not necessarily produce a peak in the susceptibility $\chi(\mathbf{q})$ that leads to the CDW instability. Large contributions to $\chi(\mathbf{q})$ are expected when large portions of the FS are spanned by a

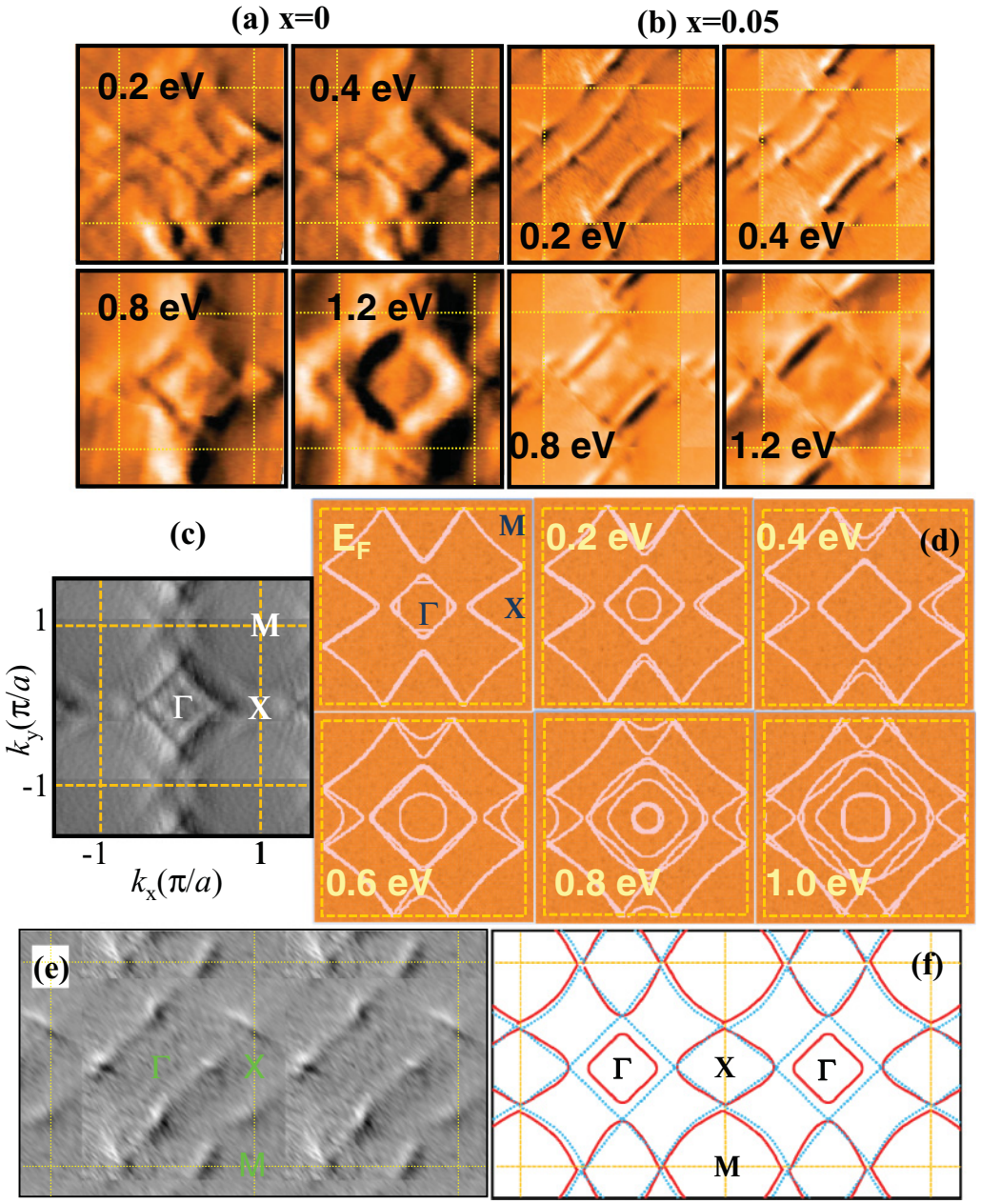

FIG. 2. (Color online) (a) First derivatives of the constant energy (CE) map of $CeTe_2$ with the increasing binding energy (BE) between 0.2 and ∼1.2 eV (BE = $|E_i|$). (b) Similarly for $CeTe_{1.95}Sb_{0.05}$; dotted lines denote the BZ. (c) Experimental CE map of $CeTe_2$ for BE = 1.0 eV. (d) Calculated CE map of $CeTe_2$ as a function of BE. (e) Experimental FS map of $CeTe_{1.95}Sb_{0.05}$, shown in the periodic zone scheme. (f) Comparison of the experimental FS map (blue dotted lines) and calculated FS map (red solid lines).

given wave vector **q** ("nesting") or from the parallel bands spanned by a **q** vector ("volume effects").[21] According to band calculations, there are two possible FS nesting vectors, one parallel to Γ-X and the other parallel to Γ-M for both $LaTe_2$[5,7] and $CeTe_2$.[7] As shown in Fig. 3, in the case of $CeTe_2$, the effects of the FS nesting seem to be realized better for $\mathbf{q} = (1/4,1/4,0) = M/2$ than for $\mathbf{q} = (1/2,0,0) = X$. However, $\chi(\mathbf{q})$ is estimated to be higher at $\mathbf{q} = X$ for both $LaTe_2$ and $CeTe_2$.[5,7] This feature supports the claim by Johannes and Mazin.[20]

In real systems, the CDW transition occurs only when there exists a soft phonon mode at a specific $\mathbf{Q}_{CDW}$. Hence the existence of a soft phonon mode at a specific **q** is the direct evidence of the CDW transition. The phonon softening is described by the renormalization of the phonon frequency by the electron-phonon (EP) interaction (the so-called Kohn anomaly):

$$\omega^2(\mathbf{q}) = \Omega^2(\mathbf{q}) - |\tilde{g}_{ep}(\mathbf{q})|^2\chi(\mathbf{q}), \quad (1)$$

where $\omega(\mathbf{q})$, $\Omega(\mathbf{q})$, and $\tilde{g}_{ep}$ correspond to the renormalized and bare phonon frequencies and the EP coupling parameter, respectively. Note that, when the phonon softening occurs, $\omega^2(\mathbf{q})$ becomes negative. In order to check the existence of a soft phonon mode in $CeTe_2$, we have calculated the phonon

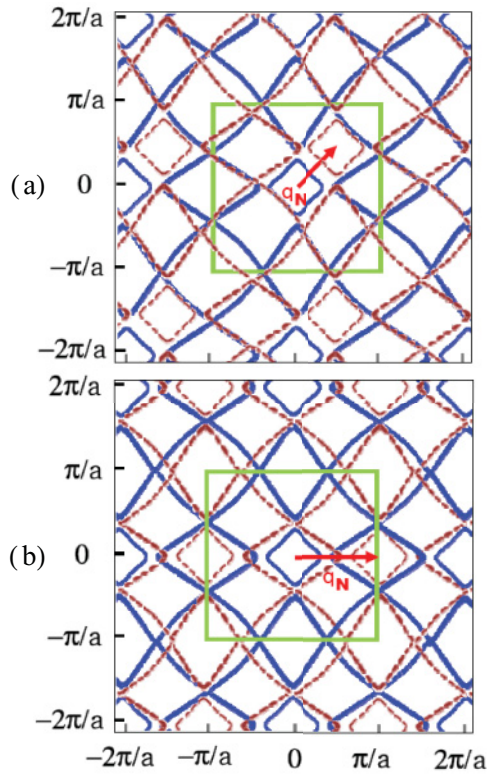

FIG. 3. (Color online) (a) Fermi-surface nesting, designated by the translational vector $\mathbf{q_N} = (1/4,1/4,0) = M/2$ for $CeTe_2$. (b) Similarly for $\mathbf{q_N} = (1/2,0,0) = X$.

dispersion $\omega(\mathbf{q})$ for $LaTe_2$ for simplicity.[16] Indeed, as shown in Fig. 4, the calculated $\omega^2(\mathbf{q})$ exhibits negative values near X, reflecting the phonon softening at $\mathbf{q} \approx X$. This finding demonstrates that $\mathbf{Q}_{CDW}$ in $CeTe_2$ corresponds to $\mathbf{q} \approx X$. In fact, the CDW modulation vector along Γ-X is also seen in $CeTe_3$, which is a similar CDW system to $CeTe_2$.[12] $\mathbf{Q}_{CDW} \approx X$ for $CeTe_2$ is smaller than $\mathbf{Q}_{CDW} \approx 1.4X$ for $CeTe_3$, which is consistent with a smaller number of hole carriers in $CeTe_2$ (nominally 1.0 in $CeTe_2$ versus 1.5 in $CeTe_3$).

In Fig. 5, we have compared the ARPES intensity plots of $CeTe_2$ with the calculated band structures, obtained for the non-CDW lattice. The left-hand sides of Figs. 5(a) and 5(b) provide the ARPES data of $CeTe_2$ along Γ-M in two

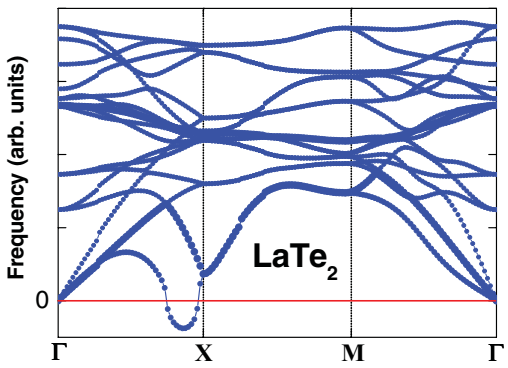

FIG. 4. (Color online) Phonon dispersion $\omega(\mathbf{q})$ of undistorted $LaTe_2$. Negative $\omega(\mathbf{q})$ here represents the imaginary part of the phonon frequency. Phonon softening occurs at $\mathbf{Q}_{CDW} \approx X$ [$\omega^2(\mathbf{Q}_{CDW}) < 0$].

different paths, along A and along D, respectively, as shown in Fig. 5(g). These ARPES intensity plots were made by taking second derivatives of the ARPES data, obtained with $h\nu \approx$ 104 eV. The experimental band structures of $CeTe_{1.95}Sb_{0.05}$ (not shown here) are found to be essentially the same as those of $CeTe_2$ without a noticeable energy shift within the instrumental resolution.[17] Many dispersive bands, observed clearly in ARPES, indicate the good quality of the samples employed in this study. The overall band structures of Figs. 5(a) and 5(b) are similar to each other.

A very good agreement is found between ARPES and calculations in both the dispersive feature and the energy positions of the bands below −0.6 eV. However, some discrepancies are also observed. The differences between two seem to arise from (i) the band-folding effect due to the increased unit cell [see Fig. 1(b)] or (ii) differences in the topography of the cleaved surfaces.[22] The band-folding effect is clearly seen in the calculated band structures, shown on the right-hand sides of Figs. 5(a) and 5(b), where the shadow bands are separated out from the main bands in the larger BZ by utilizing the band-unfolding scheme.[15] In Fig. 5(a), the wide in-plane Te(1) $5p$ band starting from M at ∼−6.2 eV to near Γ (∼0.2M) at E_F is prominent, while, in Fig. 5(b), the in-plane Te(1) $5p$ band starting from M at ∼−6.0 eV to Γ' at ∼−4.5 eV and then to near M (∼0.7M) at E_F is pronounced. In fact, the latter is seen as a dim shadow band in Fig. 5(a), and vice versa in Fig. 5(b). The main and shadow bands in Fig. 5(a) produce the bright inner FS and the dim outer FS in the first BZ (top BZ) of Fig. 5(g), respectively.

Figures 5(a) and 5(b) reveal that some of the calculated bands are missing in ARPES. In particular, the E_F-crossing bands near Γ and M, in theory, originating from Te(1) $5p$ states, are not observed clearly in ARPES, but only dim features are barely seen in Figs. 5(a) and 5(b). In order to see the bands near E_F more clearly, the ARPES intensity plots in the vicinity of E_F are shown in Figs. 5(c)–5(f). Figures 5(c)–5(e) show the near-E_F raw ARPES spectra of $CeTe_{1.95}Sb_{0.05}$ along E and those of $CeTe_2$ along A and along D in the BZ, respectively. Figure 5(f) shows the stack of momentum distribution curves (MDCs), corresponding to the constant energy cuts through the ARPES intensity plots shown in Fig. 5(e).

The band crossing through E_F is clearly observed in Fig. 5(c). These states are expected to produce the FSs at the corresponding $\mathbf{k}_F$ values.[23] On the other hand, in Figs. 5(d) and 5(e), there are bands approaching E_F, but their spectral intensities die away as they approach E_F. The expected E_F-crossing positions in ARPES agree very well with those in the calculated bands for the non-CDW phase of $CeTe_2$ [see Figs. 5(a) and 5(b)], which have mainly Te(1) $5p$ character.[7] Two bands near Γ (∼0.2M) and M (∼0.7M) in Fig. 5(d) would produce the inner bright FS and outer dim FSs, respectively, along Γ-M in the first BZ [see Fig. 5(g)]. The much weaker spectral weight of the band near M in Fig. 5(d), as compared to that near Γ, is attributed to its shadow band nature. Similarly, the band near M (∼0.7M) in Fig. 5(e) would produce the larger FS along Γ'-M in the second BZ [see Fig. 5(g)].

The vanishing spectral intensity near E_F is considered to be related to the opening of the CDW gaps in some part of the FSs. This feature is revealed more clearly in Figs. 5(h)

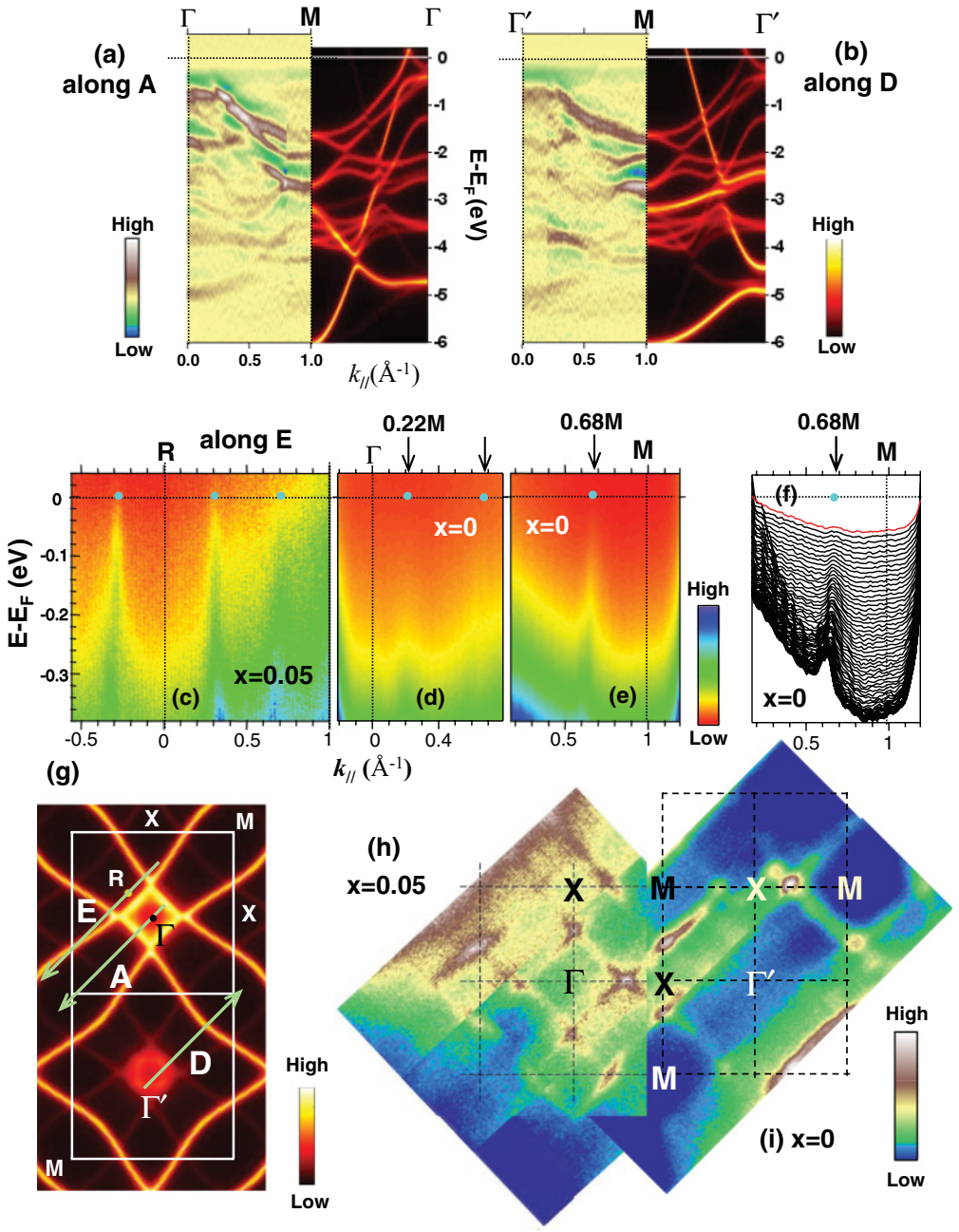

FIG. 5. (Color online) (a) ARPES along A (Γ-M), with the calculated band structures along M-Γ on the right, which is attached as a mirror image. (b) Similarly for along D (Γ'-M). (c) Near-E_F ARPES intensity plots of $CeTe_{1.95}Sb_{0.05}$ along E. (d) Near-E_F ARPES of $CeTe_2$ along A (Γ-M) in the first BZ. (e) Near-E_F ARPES of $CeTe_2$ along D (Γ'-M) in the second BZ. (f) Stack of MDCs, corresponding to (e). Top and bottom MDC curves corresponding to $E_i = 0$ eV (E_F) and -0.4 eV, respectively. (g) Unfolded FS in the extended BZ, where two different Γ-M paths, i.e., along A and D, are indicated. Note that the shadow bands and the corresponding FS are barely seen. (h) Experimental FS map of $CeTe_{1.95}Sb_{0.05}$ in the first BZ. (i) Similarly for $CeTe_2$ in the second BZ; in (h) and (i), Γ and Γ' denote the Γ points in the first BZ and the second BZ, respectively.

and 5(i), which show the experimental FS maps of the first BZ and the second BZ, respectively, obtained by integrating $E_F \pm 100$ meV. These are not the derivative data, but the raw data. The inner FS near Γ is certainly observed in Fig. 5(h), while the outer diamond FS is very weak. In contrast, the inner diamond FS near Γ' is hardly seen in Fig. 5(i), but the outer diamond FS is apparent. In view of the calculated FSs in Fig. 5(g), such differences can be interpreted as the fact that the FSs in Fig. 5(h) correspond to those in the first BZ, whereas the FSs in Fig. 5(i) correspond to those in the second BZ. Note that, in Figs. 5(d) and 5(h), the spectral intensity near M is almost vanishing, resulting in an intermittent outer diamond FS.[24] This region would correspond to the **k** points where CDW gaps open. Therefore the diminishing feature in Figs. 5(d) and 5(e) reflects the opening of the CDW gap in some part of the FS. One can estimate the size of the CDW

energy gap as being $E_g \simeq 50$ meV on the FS around M, in agreement with our previous finding in a different ARPES study.[2]

IV. CONCLUSIONS

In conclusion, the FS measured by ARPES agrees very well with the calculated FS for the undistorted $CeTe_2$ both in shapes and sizes, and the E_F-crossing metallic states are clearly observed in ARPES. We have found the following answers to the questions addressed in the beginning: (i) Ce $4f$ states have a minor contribution to the CDW formation in $CeTe_2$, while the carriers near E_F have mainly the Te(1) $5p$ character; (ii) the band folding originating from the interaction with Ce-Te(2) layers produces the shadow bands and the corresponding FSs, which have very weak spectral weight; and (iii) the CDW modulation vector is estimated to be $\mathbf{Q}_{\mathrm{CDW}} \approx X$. The CDW gap opens in some part of the FS, with the size of the CDW energy gap being $E_g \simeq 50$ meV around M.

ACKNOWLEDGMENTS

This work was supported by the National Research Foundation of Korea (NRF) (Contracts No. 2011-0022444 and No. 2009-0079947) and also by the Korea Institute of Science and Technology Information supercomputing center (Grant No. KSC-2011-C2-36). Y. S. K. acknowledges the NRF grant under Contracts No. 2006-2002165 and No. 2009-0078025. Pohang Light Source is supported by Pohang University of Science and Technology and the Ministry of Education, Science, and Technology in Korea.

*kangjs@catholic.ac.kr
†bimin@postech.ac.kr

[1] M. H. Jung, A. Alsmadi, H. C. Kim, Y. Bang, K. H. Ahn, K. Umeo, A. H. Lacerda, H. Nakotte, H. C. Ri, and T. Takabatake, Phys. Rev. B **67**, 212504 (2003).
[2] J.-S. Kang, C. G. Olson, Y. S. Kwon, J. H. Shim, and B. I. Min, Phys. Rev. B **74**, 085115 (2006).
[3] J. K. Burdett and S. Lee, J. Amer. Chem. Soc. **105**, 1079 (1983).
[4] J.-S. Kang, C. G. Olson, Y. S. Kwon, S. W. Han, K. H. Kim, A. Sekiyama, S. Kasai, S. Suga, and B. I. Min, J. Phys. Condens. Matter **16**, 9163 (2004).
[5] A. Kikuchi, J. Phys. Soc. Jpn. **67**, 1308 (1998).
[6] E. DiMasi, B. Foran, M. C. Aronson, and S. Lee, Phys. Rev. B **54**, 13587 (1996).
[7] J. H. Shim, J.-S. Kang, and B. I. Min, Phys. Rev. Lett. **93**, 156406 (2004).
[8] K. Stöwe, J. Alloy Compd. **307**, 101 (2000).
[9] K. Y. Shin, V. Brouet, N. Ru, Z. X. Shen, and I. R. Fisher, Phys. Rev. B **72**, 085132 (2005).
[10] T. Ito, H. J. Im, S. Kimura, and Y.-S. Kwon, J. Magn. Magn. Mater. **310**, 431 (2007).
[11] D. R. Garcia, G.-H. Gweon, S. Y. Zhou, J. Graf, C. M. Jozwiak, M. H. Jung, Y. S. Kwon, and A. Lanzara, Phys. Rev. Lett. **98**, 166403 (2007).
[12] V. Brouet, W. L. Yang, X. J. Zhou, Z. Hussain, N. Ru, K. Y. Shin, I. R. Fisher, and Z. X. Shen, Phys. Rev. Lett. **93**, 126405 (2004); V. Brouet, W. L. Yang, X. J. Zhou, Z. Hussain, R. G. Moore, R. He, D. H. Lu, Z. X. Shen, J. Laverock, S. B. Dugdale, N. Ru, and I. R. Fisher, Phys. Rev. B **77**, 235104 (2008).
[13] B. H. Min, H. Y. Choi, and Y. S. Kwon, Physica B **312–313**, 203 (2002); **312–313**, 205 (2002).
[14] H. J. F. Jansen and A. J. Freeman, Phys. Rev. B **30**, 561 (1984); P. Blaha *et al.*, computer code WIEN2k, Technical Universität Wien, 2001.
[15] W. Ku, T. Berlijn, and C.-C. Lee, Phys. Rev. Lett. **104**, 216401 (2010).
[16] P. Giannozzi, S. Baroni, N. Bonini, M. Calandra, R. Car, C. Cavazzoni, D. Ceresoli, G. L. Chiarotti, M. Cococcioni, I. Dabo, A. D. Corso, S. de Gironcoli, S. Fabris, G. Fratesi, R. Gebauer, U. Gerstmann, C. Gougoussis, A. Kokalj, M. Lazzeri, L. Martin-Samos, N. Marzari, F. Mauri, R. Mazzarello, S. Paolini, A. Pasquarello, L. Paulatto, C. Sbraccia, S. Scandolo, G. Sclauzero, A. P. Seitsonen, A. Smogunov, P. Umari, and R. M. Wentzcovitch, J. Phys. Condens. Matter **21**, 395502 (2009).
[17] The ground state and the electronic structures of $CeTe_2$ remain almost the same in $CeTe_{1.95}Sb_{0.05}$ in this energy scale, since the Sb concentration in $CeTe_{1.95}Sb_{0.05}$ is very low (2.5%).
[18] M. Lavagnini, A. Sacchetti, L. Degiorgi, K. Y. Shin, and I. R. Fisher, Phys. Rev. B **75**, 205133 (2007).
[19] K. E. Lee, C. I. Lee, H. J. Oh, M. A. Jung, B. H. Min, H. J. Im, T. Izuka, Y. S. Lee, S. Kimura, and Y. S. Kwon, Phys. Rev. B **78**, 134408 (2008).
[20] M. D. Johannes and I. I. Mazin, Phys. Rev. B **77**, 165135 (2008).
[21] M. Gupta and A. J. Freeman, Phys. Rev. Lett. **37**, 364 (1976).
[22] All the cleaved surfaces were mirror shiny but had many stepped planes. Due to a finite acceptance angle of the electron analyzer and a different topography of a cleaved surface, each cleaved surface is expected to have a different yield.
[23] In the energy distribution curves (EDCs), the photoemission peaks that cross E_F were not observed clearly. Nevertheless, the E_F-crossing of these bands is supported by the slope of these bands.
[24] The polarization effect of the incident light is not likely the origin of an intermittent feature of the outer FS, since this feature is common for all four sides of the outer diamond.